Invited paper

Fracture of Reinforcing Steels in Concrete Structures Damaged by Alkali-Silica Reaction —Field Survey, Mechanism and Maintenance—

Toyoaki Miyagawa[1], Kaoru Seto[2], Kazunori Sasaki[3], Yasuhiro Mikata[4], Kazuhiro Kuzume[5] and Toshikazu Minami[6]

Received 30 June 2006, revised 29 September 2006

Abstract

Instances of reinforcing steel fracture in concrete structures damaged by the alkali-silica reaction (ASR) have been discovered recently in Japan. As long as reinforcing steels are not broken due to ASR-caused expansion, the safety of a structure is considered not to be seriously compromised. However, the safety of a structure becomes questionable when the confinement of concrete becomes degraded due to the fracture of reinforcing steel bars. Therefore, it is important to clarify the mechanism of the fracture of reinforcing steel bars and develop methods for detecting steel bar fractures and strengthening concrete structures damaged by ASR.

This paper describes the fracture of reinforcing steels in the case of concrete structures damaged by ASR in the Kansai area in Japan. It then introduces the results of investigation on the fracture mechanism, nondestructive testing methods, and repair and strengthening methods for damaged concrete structures.

1. Introduction

Although only rare instances of Alkali-Silica Reaction (ASR) affecting concrete structures in Japan had been reported prior to 1970, this type of deterioration was discovered in the bridge piers of the Hanshin Expressway in 1982 and thereafter additional cases have been confirmed in many types of structures, such as bridge piers, protective walls, and levees, that use crushed andesite as the concrete aggregate.

The Ministry of Construction and the Japan Concrete Institute launched nationwide surveys and began investigating countermeasures, eventually proposing an ASR testing method for aggregate measures to control ASR damage, and methods for the assessment, diagnosis, and repair of structures damaged by ASR.

In 1986, a test method and ASR control measures including the use of non reactive aggregate, blast furnace slag cement, low alkali type cement and the control of the total alkali content were established, and since 1990 there has been few ASR cases reported in newly constructed structures.

On the other hand, structures damaged by ASR that were constructed in the 1970s and 1980s have been actively repaired with the application of surface coating to prevent moisture penetration from the outside. However, it has become clear, in some cases, that preventing moisture penetration fails to completely stop the expansion of ASR.

In the latter half of the 1990s, fractures in reinforcing steel bars were found. The Committee on the Countermeasures for the Damage Due to Alkali-Silica Reaction (chaired by Prof. Toyoaki Miyagawa, Kyoto University) was established under the Concrete Committee, Japan Society of Civil Engineers, to investigate the current status and the mechanism of reinforcing steel bar fractures, the assessment of the safety of structures, and repair and strengthening. Additionally, the Highway Bridge Maintenance Manual (draft), which addresses the problem of steel bar fractures, was prepared by the Ministry of Land, Infrastructure and Transportation, and the nationwide investigation of ASR-caused fractures is still going on (Concrete Library-124, 2005).

Japan currently counts some 30 ASR-damaged structures, including highway and railroad bridges, confirmed to have steel bar fractures. Andesite type reactive aggregate, which is very prone to volume expansion, was used as the concrete material at the locations where these steel bar fractures occurred. Additionally, steel bar fractures occurred at many bent sections of steel bars in pier beams, and similar cases have been reported to occur in footings. The data shows that ASR-caused deterioration is influenced by weather (rain water, sunlight, etc.) and tends to be particularly severe at places where the amount of steel bars is relatively small (**Fig. 1**). The results of investigations targeting ASR-damaged structures in the Kansai area of Japan are presented below.

[1]Professor, Department of Civil & Earth Resources Engineering, Kyoto University, Japan.
E-mail:miyagawa@sme.kuciv.kyoto-u.ac.jp
[2]Director, Osaka National Highway Works Office, Ministry of Land, Infrastructure and Transport, Japan.
[3]Hanshin Expressway Co. Ltd., Japan.
[4]Assistant Professor, Department of Civil Engineering and Urban Design, Osaka Institute of Technology, Japan.
[5]Kokusai Structural Engineering Corp., Japan.
[6]Shinko Wire Co. Ltd., Japan.

2. Fracture of reinforcing steel bars in highway bridge damaged by ASR

2.1 Example of steel bar fracture

The examined concrete member with steel bar fractures is a PC beam of a T-shaped pier that was constructed in 1979. This pier had been repaired twice applying surface protective coating and crack injection in 1989 and 1992 because of the serious development of ASR-caused cracking.

During an investigation in 1999, the compressive strength of the core specimen was approximately 10 to 15 N/mm^2 lower than the specified concrete strength, 35 N/mm^2. Young's modulus of this core was down to about half the usual value of sound concrete. In order to confirm the soundness of the steel bars, chipping inspection of the corner of the beam crown (**Fig. 2**) was conducted. Fractures were discovered at the bent sections of the stirrups (**Fig. 3**).

One of the features of the cracks at the locations in concrete where the steel bars were fractured was that extensive cracks perpendicular to the direction of the reinforcing steel bars had developed at locations where the amount of steel bars was too small to confine concrete expansion. The locations with a smaller amount of stirrups tended to fracture more. Bent main steel bars fracture at beam ends, where weather attacks are more severe, were found when the deterioration caused by ASR had significantly developed.

2.2 Examples of inspection of piers damaged by ASR

The rate of ASR expansion depends largely on environmental factors such as the presence of moisture. Therefore, it is necessary to adequately consider and assess the condition of the structure because, in many cases, the degree of deterioration differs depending on the location of the structure. At present, the ASR process has not been completely elucidated. As a result, the quantitative estimation of future deterioration is difficult, and so is determining which measures should be taken when. In carrying out the maintenance and management of structures identified as suffering from ASR-caused deterioration, repair and strengthening actions must be decided on a case-by-case basis for each individual structure. It is also necessary to conduct suitably designed inspections according to an appropriate schedule. Follow-up inspections are also needed to evaluate the effect of the measures taken. The collection and analysis of the data obtained through the above processes is essential for rationally maintaining and managing ASR-damaged structures.

The Hanshin Expressway Company Limited launched a field investigation to determine the actual condition of ASR in 1982. The inspections carried out include visual inspection, measurement of crack width, pier dimensions, ultrasonic wave velocity, compressive strength, modulus of elasticity, remaining expansion capacity, and moisture content of concrete (Kuzume *et al*. 2004).

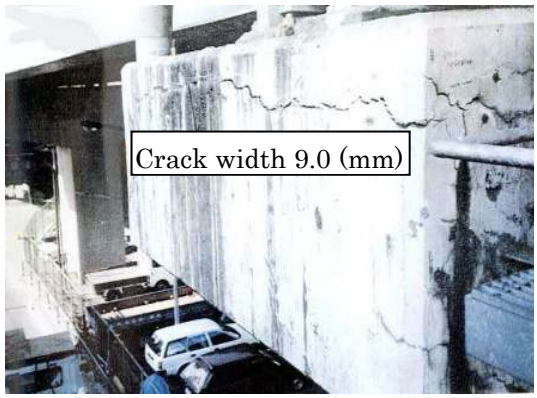

Fig. 1 Example of pier damage.


Fig. 2 Chipping inspection of pier beam.


Fig. 3 Example of fractured steel bar.

Figure 4 shows the increase in the average width of the specified cracks in the piers over time. Most of the cracks remained about 1 mm in width until about 20 years after the completion of the piers, but some cracks developed to exceed 3 mm in some piers. Still other cracks began suddenly increasing in width at a given time. **Figure 5** shows the length expansion at each location. The rate of increase in dimensions differed according to the line of traverse, but continued to increase constantly on the lower surface of the beam, where the rate was the largest.

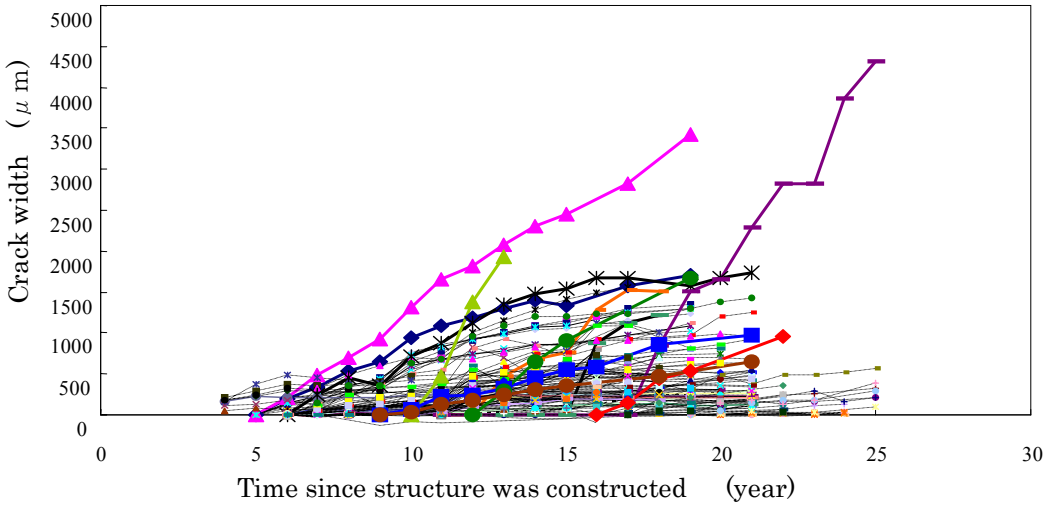

Fig. 4 Example of variations in crack width.

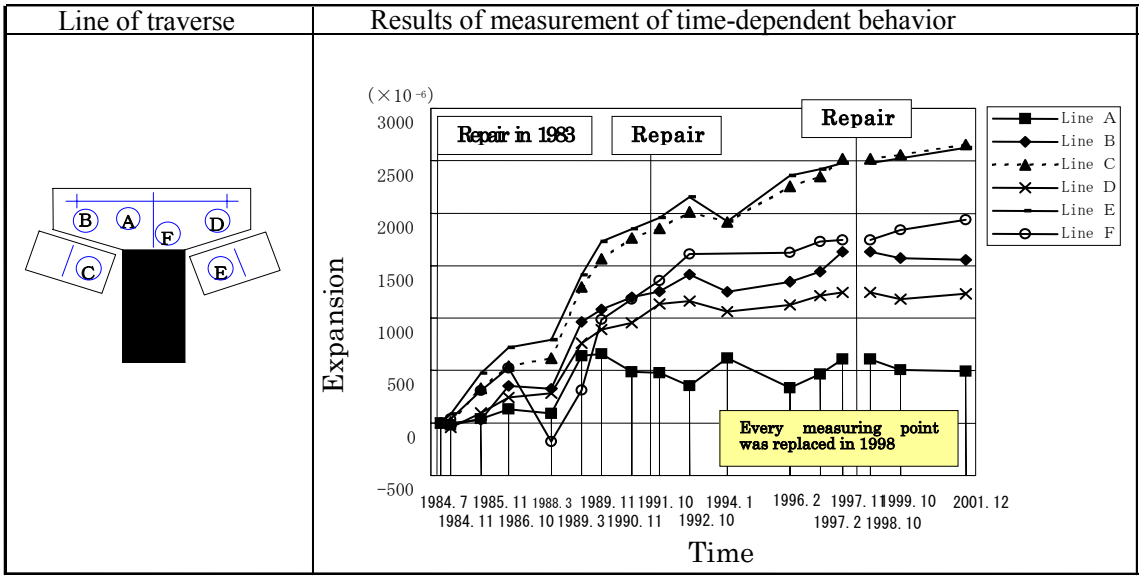

Fig. 5 Examples of increases in pier dimensions.

3. Fracture mechanism of reinforcing steel bars

In order to investigate the cause of damage to the steel bars in bridge piers damaged by ASR, material tests were conducted on the steel bars (Sasaki *et al.* 2005). First, to examine the influence of bending, bending tests and analyses were carried out (Iwakawa *et al.* 2003). Next, to study the effect of the environment, accelerated damage tests (stress corrosion cracking, hydrogen embitterment) and hydrogen absorption tests were conducted.

New specimens of the steel bar (JIS G 3112 SD295A, D16, currently available commercially) used were obtained from the same manufacturer that supplied the actual steel bars that suffered damaged.

3.1 Chemical composition and physical properties of steel bar

Table 1 lists the chemical composition and physical properties of a steel bar that was taken from the concrete along with those of a new specimen. There are differences in the chemical composition of the damaged and new specimens, notably the Si, Mn, Cu, and Cr content,

but these may be the result of differences in the composition of the steel scraps used for manufacturing the reinforcing steel. The amount of N, which largely influences strain aging, is approximately 0.01% for both specimens, and they both contain the same small amount of Al, which stabilizes N as nitride. As for the influence of N and Al on strain aging, it has been made clear that steel bars become harder due to strain aging when the amount of N is greater than 0.007%, and it is possible to retard the start of aging if approximately 0.1% of Al is added. All the test specimens had more than approximately 0.01% of N and 0.002% of Al, and thus there was a high incidence of materials developing strain aging.

Both the damaged and new specimens satisfy the Japanese industrial standard values for mechanical properties of SD295A (D16), which exhibited much damage in existing damaged bridges. The damaged specimen shows slightly higher values than the new specimen obtained in the current market. Optical microscopic observation of used specimens revealed a ferrite-pearlite structure equivalent to 0.2% C, which is common. At the base of the ribs of the deformed bar, the new specimen have a larger radius where the shape changes compared to the damaged, old specimen, which constitutes an improvement against stress concentration.

3.2 Bending test

Test steel bars were bent with bending radii of 2 d, 1.5 d, and 1 d, where "d" is the nominal diameter of the steel bar, using a bender as shown in **Fig. 6**. Magnetic particle tests and tensile tests were conducted on the specimens.

3.2.1 Fluorescent magnetic particle test

Cracking damage to bent steel bars developed on the inner bending surface as wrinkles occurred on this surface. Steel bars with bending radii of 2 d and 1 d were bent 90 deg., and the presence of cracks on the inner bending surface was investigated. The crack condition of the specimens as the result of a fluorescent magnetic particle test is shown in **Fig. 7**. The specimen with 1 d bending radius clearly displays cracks in white, whereas the specimen with 2 d bending radius presents a somewhat blurred image indicating no cracks. **Figure 8** shows a cross-section of the bent corner. The presence of cracks of approximately 15 μm was confirmed in the specimen with the 1 d bending radius through Scanning Electron Microscope (SEM) observation, and no cracks were found in the specimen with the 2 d bending radius, per the results of fluorescence magnetic particle tests.

3.2.2 Tensile test

Tensile tests were conducted using new steel bars 80 cm long and bent 90 deg. as shown in **Fig. 9**. Both ends of each bar were bent 45 deg. to hold the specimen using two opposing chucks, and each bar was ruptured under tension force. Some bent samples were heat-treated to investigate the influence of strain aging. For this purpose, heat treatment at 150°C for 10 min. was provided to simulate the strain aging of a one-year period. (Hundy 1954)

The results of the tensile test are shown in **Table 2**. Without the aging treatment, the tensile strength of the specimen with 1 d bending radius that developed cracks was reduced to approximately half the value of the unbent specimen, and the strength was further reduced when the bar was treated for strain aging. Other bent specimens tested showed strength almost equal to that of the unbent specimen.

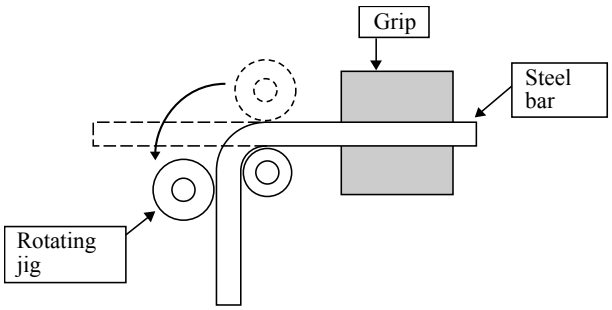

Fig. 6 Layout for bending steel bars.

Table 1 Chemical composition (mass%) and mechanical properties.

	Chemical Composition										Mechanical Properties		
	C	Si	Mn	P	S	Cu	Ni	Cr	Al	N	Yield Point MPa	Tensile Strength MPA	Elongation %
Damaged sample from field	0.25	0.22	0.70	0.024	0.035	0.26	0.09	0.11	0.002	0.0107	356	550	23
New sample from market	0.21	0.06	0.41	0.028	0.046	0.46	0.11	0.36	0.002	0.0122	342	504	25
Requirement in JIS G 3112 SD295A	-	-	-	Less than 0.05	Less than 0.05	-	-	-	-	-	More than 295	440-600	More than 16

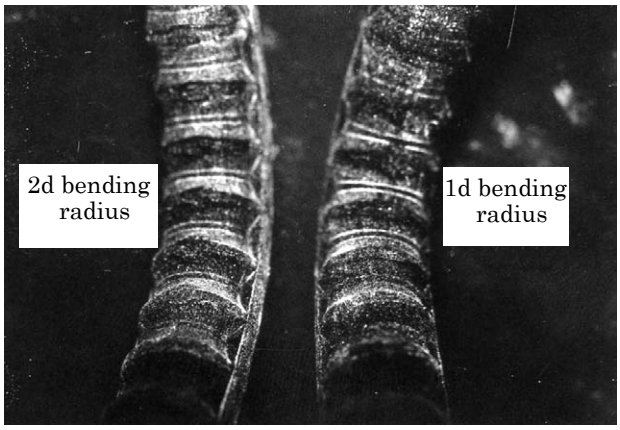

Fig. 7 Condition of crack (fluorescent magnetic particle inspection).

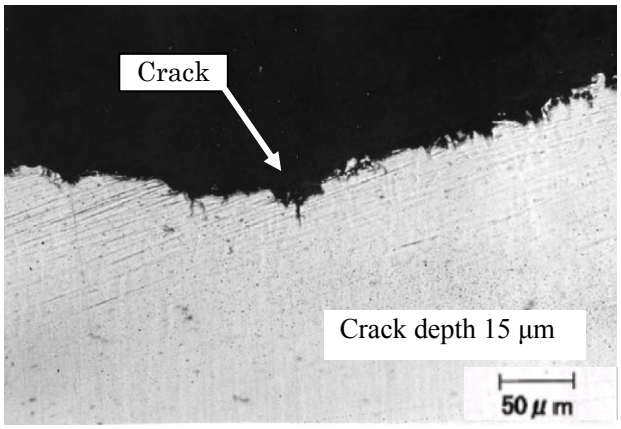

Fig. 8 Vertical section of inner part of bend (1d bending radius).

Figure 10 shows an exterior view of fractures after the tensile test, and **Fig. 11** shows the fracture surface of the specimen viewed by SEM. The fracture surface at the bent section of the 1 d bending radius is a ductile fracture surface (in dimple forms) on concentric circles from the fracture origin, and outside this area (lower side), it is a brittle cleavage fracture surface. By contrast, specimens with 2 d and 1.5 d bending radii fractured with contraction at locations other than the bent part regardless of application of strain aging.

3.3 Bending analysis

The degree of the initial cracking during bending of a steel bar is considered largely influenced by the shape of the steel bar rib and bending radius. Therefore, bending tests and Finite Element Method (FEM) analysis were used to investigate the sensitivity to fracture in relation to differences in the shape of ribs and bending radius. The sample steel bars that were used were SD295A (D16).

3.3.1 Bending test

Steel bars were bent using a steel bender with radii, r, of 16 mm (1.0 d), 24 mm (1.5 d), 30 mm (1.9 d), and 40 mm (2.5d), producing four types of specimen, and the

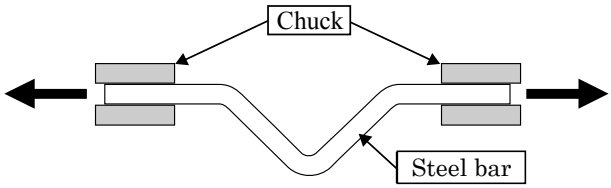

Fig. 9 Layout of tensile test.

Table 2 Tensile strength.

Bending Radius	Aging Treatment (150℃, 10 min)	
	No	Yes
No	504	-
1.0 d	249	207
1.5 d	504	492
2.0 d	494	494

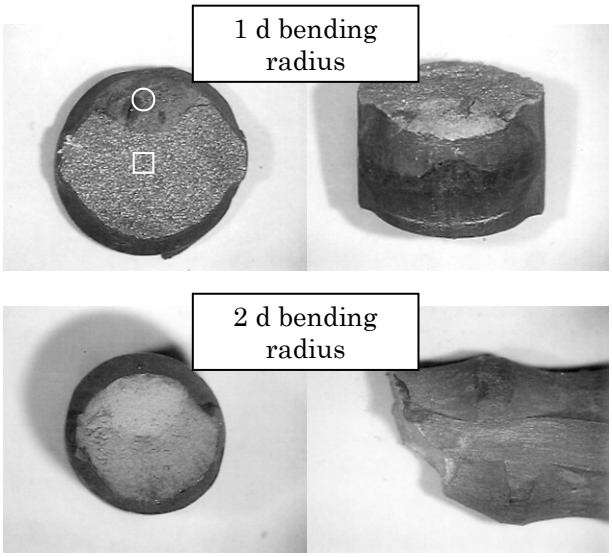

Fig. 10 Exterior view of fracture after tensile test.

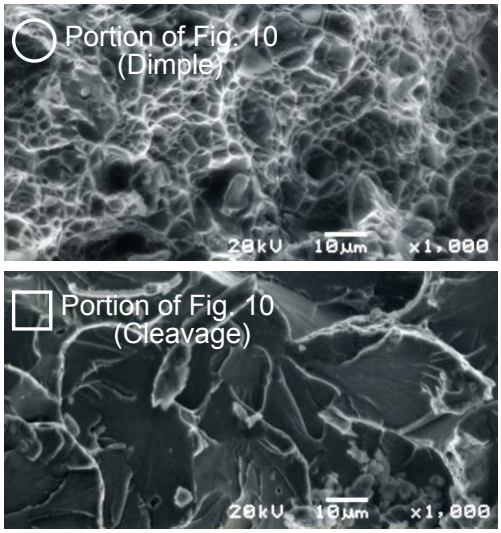

Fig. 11 Fracture after tensile test (SEM).

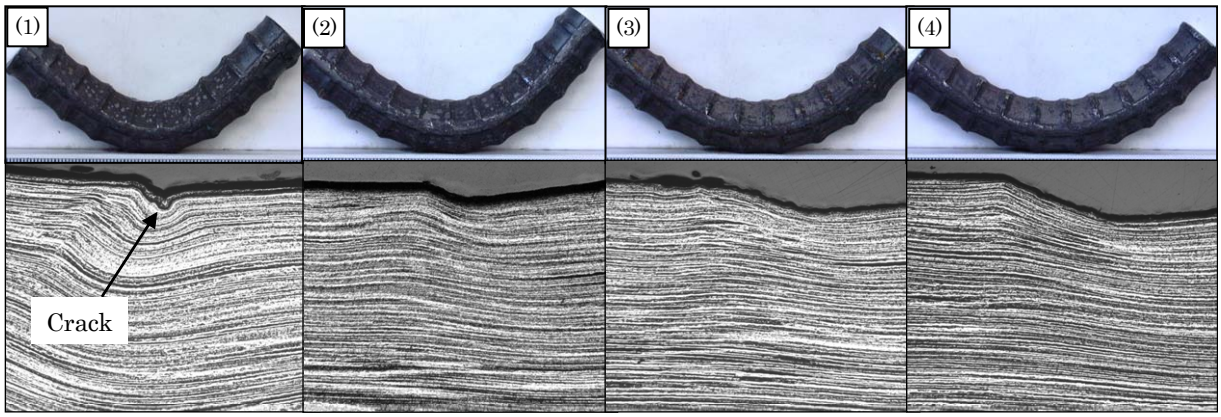

Fig. 12 Exterior view after bending and metal flow around rib base.
[(1) r = 1.0 d, (2) r = 1.5 d, (3) r = 1.9 d, (4) r = 2.5 d]

external appearance and the condition in the vertical section were examined. **Figure 12** shows the exterior views of the steel bars after bending and the metal flow conditions at the base of the ribs obtained from these examinations.

Cracking (approximate depth 50 μm) at the base of the rib on the inner surface of the bent corner was produced only in the bar with the bending radius of 1.0 d.

Ribs on the inner side of the bent corner were crushed. When the bending radii are small, characteristically, ribs get crushed easier because the number of ribs in contact with the bender is smaller (four ribs for 1.0 d radius bending).

Ribs on the outer side of the bent corner were deformed, being pressed against the rotating jig. Bars bent at the 1.0 d radius showed cracks in places where the metal flow was sharply bent and significantly curved. However, metal flow discontinuity due to cracking was not observed.

3.3.2 FEM analysis of bent section

The shapes of the bars that were analyzed were round steel (without ribs), current shape, and old shape. A computer model reproduced the steel bar used for the experiment to represent the current shape for FEM analysis. Another computer model reproduced the steel bar damaged in the bridge to represent the old shape. The computer models for steel bars are shown in **Fig. 13**.

The bending mode was reproduced using a steel bender, and four bending radii, 1.1 d, 1.5 d, 2.0 d, and 2.3 d, were analyzed. For computer analysis, Young's modulus was 210 000 MPa, Poisson's ratio was 0.3, and the yield stress was 305 MPa, respectively, as usual values. The analysis program ABAQUS/STANDARD Ver. 6.3 was used.

Since the steel bars were extremely deformed (non-linear) by the bending operation, the amount of strain was evaluated using the value of equivalent strain. **Figure 14** shows the relationship between the maximum equivalent strain and bending radius at the base of a rib.

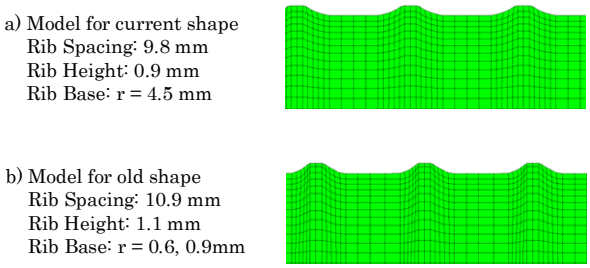

Fig. 13 Computer model for steel bar shape.

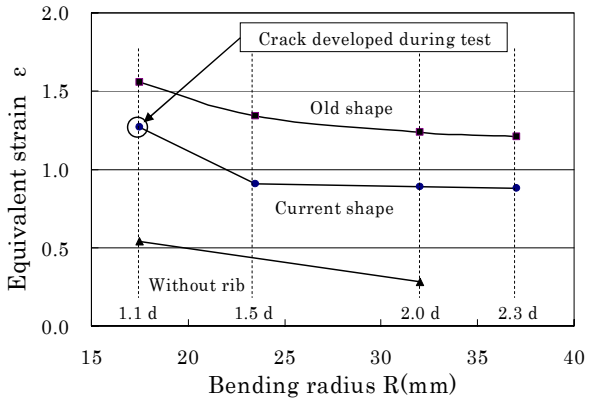

Fig. 14 Relationship between maximum equivalent strain and bending radius.

The following results were obtained from the analysis.

For steel bars with ribs, the maximum equivalent strain is generated at the base of the rib on the inner surface. For steel bars without ribs, the maximum equivalent strain was on the inside and outside the bent section. The values were 0.54 for the 1.1 d radius and 0.28 for the 2.0 d radius. The maximum equivalent strain was 1.27 for the current shape steel bar with the bending radius of 1.1 d. When the radius was more than 1.5 d, the value was less than 0.91. According to these bending test results, cracks seemed to develop when the

strain exceeded 0.91 because they were observed only at the bases of the ribs with 1.1 d radius bending.

In the case of old shape steel bars, the maximum strain exceeded 1.0 for all bending radii, and of special note here is the bar with a radius 1.1 d that resulted in an extremely large strain, 1.56. The steel with the 2.0 d bending radius showed a strain of 1.24, which is almost equivalent to 1.1 d for the current shape steel bar.

However, the analytical results may quantitatively show slightly larger values of strain because there is no clearance between the steel bar and the rotating jig of bender as the operation is conducted under an ideal contact condition for the computer model, making it more severe than the actual bending work.

3.4 Stress corrosion cracking and hydrogen embrittlement

In order to determine whether delayed deterioration (stress corrosion cracking and hydrogen embrittlement) has anything to do with the damage to steel bars, loading tests were conducted in a corrosive environment. Steel bars available in the current market, SD295A (D16), were used as sample specimens, and four pieces were prepared: bars with bending radii of 1.0 d, 2.5 d, one bar without bending, and one bar with bending radius of 2.5 d heat-treated at 150°C for 10 min. The specimens were bent back to be set on the testing machine. A test load of 60% (60 kN) of tensile strength was applied, and this condition was maintained for 100 hrs at the longest. When the testing specimen fractured, the fracture surface and the time to failure were observed. If a specimen did not fracture, a tensile test was conducted, and a comparison was made with the tensile load before the test. The testing solutions are described below:

[Stress Corrosion Cracking]: 20wt% NH_4NO_3 aqueous solution at 100°C

[Hydrogen Embrittlement]: 20wt% NH_4SCN aqueous solution at 50°C

Table 3 shows the results of delayed deterioration tests (stress corrosion cracking and hydrogen embrittlement). Eight specimens were tested. Here, specimens that did not fracture for longer than 100 hrs. are indicated with a dash (−) mark. Samples without bending did not fracture in either test. All bent specimens fractured at early stages (6.5 hrs to 8.8 hrs) during the stress corrosion cracking test. One out of two specimens with 1.0 d bending radius fractured at 25 hrs in the hydrogen embrittlement test, but the other samples did not fracture.

The fracture surface of samples that failed during the delayed deterioration test was observed. The fractures caused by the stress corrosion cracking test of bent specimens showed no differences among the various bending radii, heat-treatment, and non-heat-treated, and they showed a similar trend.

Figure 15, which was taken with an optical microscope, is of cracks observed in the vicinity of the fracture of the 2.5 d aging sample, and it shows the condition of cracks leading to fracture. The development of cracks from the big trunk to the fine branches can be seen. This is the typical manner in which cracking takes place in stress corrosion cracking. However, this is not what happens in the field. Additionally, the cracks can be seen to proceed along the grain boundaries. The central part of the fracture was in dimples, indicating ductile failure.

Table 3 Results of constant load test.

Sample	Stress Corrosion Crack		Hydrogen Embrittlement	
No bending	-	-	-	-
1.0 d	6.5 hrs	7.7 hrs	-	25 hrs
2.5 d	7.6 hrs	7.3 hrs	-	-
2.5 d-aging	7.7 hrs	8.8 hrs	-	-

Note) - : non fracture

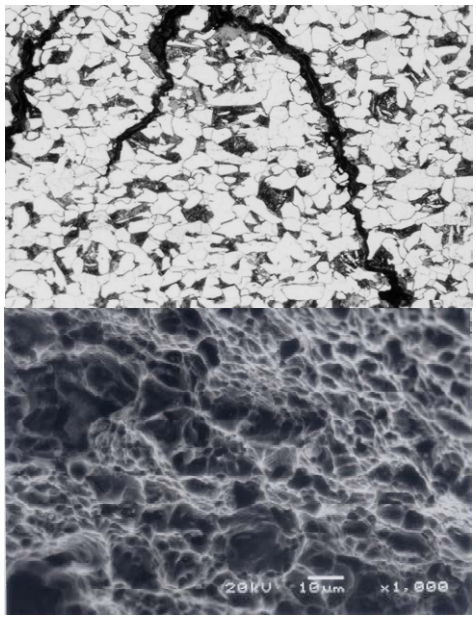

Fig. 15 Vertical section through cracks after stress corrosion cracking test and fracture surface (2.5 d aging).

Figure 16 shows the central part of the fracture of the sample with 1.0 d bending radius that failed during the hydrogen embrittlement test. The origin was the grain fracture that developed from the hydrogen embrittlement, and the center was a cleavage fracture surface.

3.5 Hydrogen absorption test

The possibility of hydrogen embrittlement was investigated by comparing the hydrogen absorbing property of SD295A (16) steel bars with different working records.

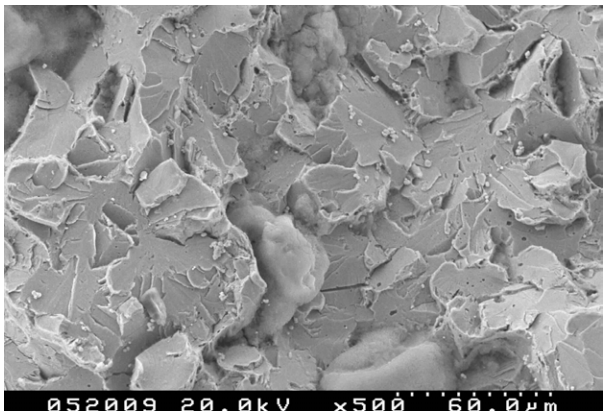

Fig. 16 Fracture surface by hydrogen embrittlement test (1 d).

Samples with three different treatments as shown below were used: (1) Straight section (unbent), (2) Bent section and (3) Bent and heat treated section (150°C for 10 min.)

From the test part of each sample, two pieces of 1.5 mm thick plate specimens were cut out from the steel bar. The hydrogen content of the steel was analyzed following hydrogen charge treatment by the electrochemical method (cathodic polarization).

Figure 17 shows the hydrogen charge treatment method using electrolysis solution of sulfuric acid (pH 2.0) with conditions of a current Density of 1 mA/cm^2 and an electrolysis time of 24 hrs.

Each specimen were washed and dried after the hydrogen charge treatment. Specimens were stored immediately at low temperature in liquid nitrogen until they were subjected to hydrogen analysis to avoid hydrogen dispersion in the normal temperature environment. Then they were weighed and quantitatively analyzed for the hydrogen content of the steel using an atmospheric pressure ionization mass analyzer (API-MS). **Figure 18** shows the general layout of the API-MS.

Experimental conditions were a controlled temperature ranging from 20 to 600°C, temperature rising rate of 12 deg./min and Argon purging gas flow rate of 1000 ml/min.

The results of hydrogen analysis after hydrogen charge treatment of each specimen are shown in **Fig. 19**. A first peak that shows a discharge peak in the 100 to 200°C range and a second peak that shows a discharge peak in the 200 to 300°C range can be observed independently. In the temperature rising hydrogen analysis, hydrogen having higher stability in steel has been observed as a discharge peak on the high temperature side. Therefore, for the steels with two peaks, the dispersing

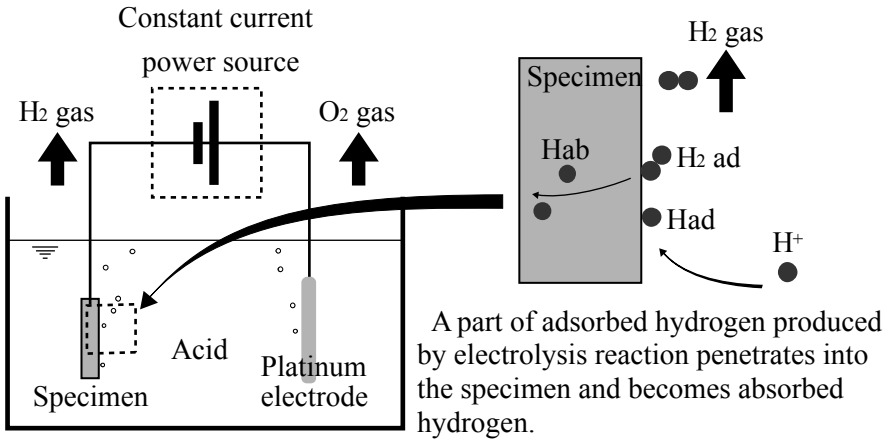

Fig. 17 Hydrogen charge treatment method.

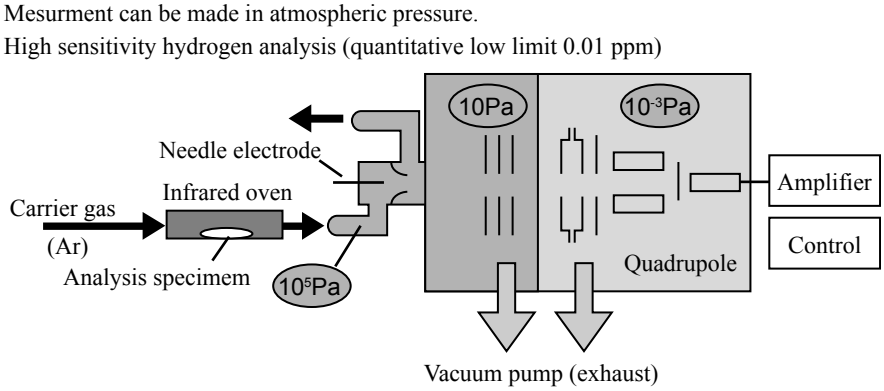

Fig. 18 Layout of API-MS.

hydrogen of the first peak largely influences the hydrogen embrittlement in steel, and the hydrogen of the second peak is believed to be the hydrogen trapped in steel.

The integrated amount of hydrogen is the least for the straight sample. The bending operation increases the absorption of hydrogen. The bent section samples in particular show a significant increasing trend of the first peak and little second peak hydrogen variation.

In comparing bent sections with and without heat treatment, no large differences are seen, and differences in hydrogen absorption amount due to strain aging are considered to be small.

In general, for high strength steel with a strength in excess of 1000 MPa, the absorption of hydrogen in the amount of approximately 0.1 ppm in a normal atmospheric corrosive environment easily leads to delayed deterioration caused by hydrogen embrittlement. The strength, estimated by hardness, of a section of bent steel is 800 MPa or higher. Therefore, due to work hardening and strain ageing , the hydrogen embrittlement sensitivity of D16 steel may be considered to increase.

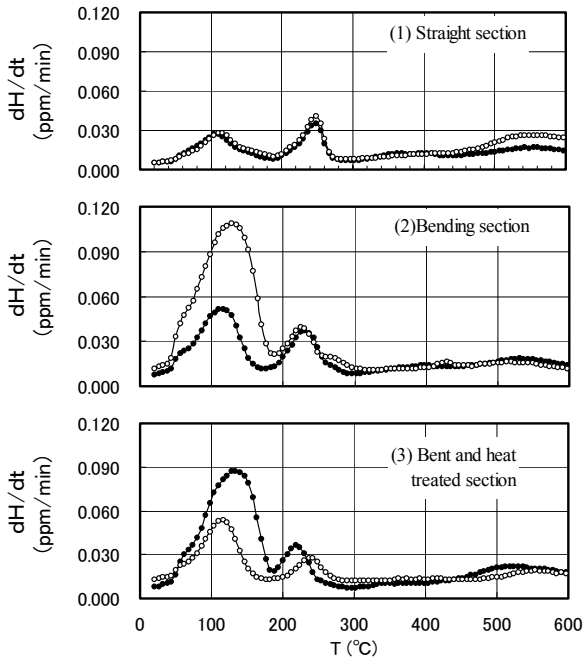

Two specimens ware tested under same condition.

Fig. 19 Results of API-MS measurement.

3.6 Presumed mechanism of damage to steel bars

Currently, an investigation is under way to determine the cause of steel bar fractures. Nationwide ASR investigations have been yielding various reports on steel bar fractures. While steel bar damages are characterized by many different conditions, some common phenomena in the Kansai area are listed below.

(1) Many cracks have developed in concrete due to ASR.
(2) Damages are present at the bent section of steel bars.
(3) The fracture condition is brittle in nature without plastic deformation (cross section reduction).
(4) The steel bars were in a corrosive environment, judging from the development of corrosion around the damaged area of the bars.
(5) The concrete is contaminated by sea sand with Cl^- used as fine aggregate.

Judging from these phenomena and conditions, the mechanism shown in **Fig. 20** is presumed as one of the scenarios explaining the cause of steel bar fracture in

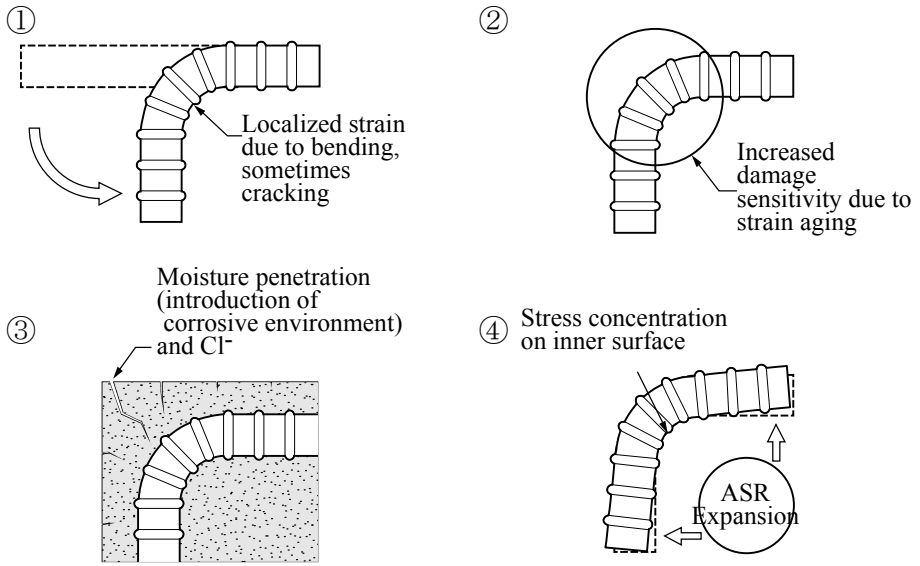

Fig. 20 Presumed mechanism of damages to steel bars.

concrete structures having significantly developed ASR deterioration.

(1) The toughness of the material decreases with increase in strength, as work hardening of the bent section takes place owing to the bending operation. At this time, cracks may develop near the base of the rib, depending on the bending radius and rib shape.
(2) Strain aging (brittleness) progresses with time, and the sensitivity to fracture increases.
(3) Moisture penetrates through cracks generated in concrete damaged by ASR. Sometimes concrete is contaminated with chloride ions from sea sand used as fine aggregate.
(4) The generation of straightening force in the steel bar develops stress concentration at fine cracks caused by the expansion force of ASR. This phenomenon initiates cracking and may lead to a fracture under certain conditions. Additionally, there is the possibility of hydrogen embrittlement due to the presence of tensile stress and a corrosive environment, and the material brittleness may progress.

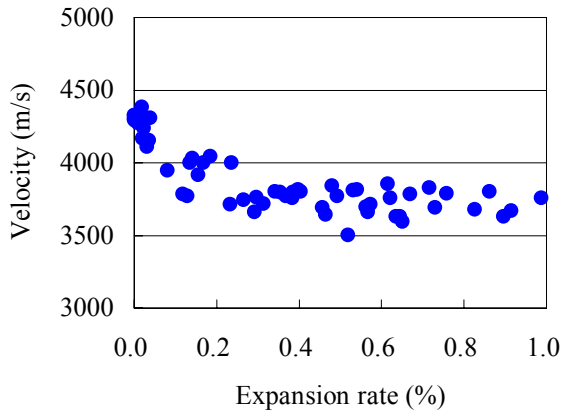

Fig. 21 Relationship between ultrasonic wave velocity and expansion.

4. Non-destructive testing of structures deteriorated by ASR

When the deterioration by ASR becomes visible, it is necessary to intermittently evaluate the presence of damage to the inner part of the structure and the progression rate of such deterioration. The use of non-destructive testing is desirable for this purpose. Methods that can be applied include the ultrasonic wave method for investigating the deterioration in concrete and the electromagnetic method for inspecting the presence of fracture in steel bars.

4.1 Ultrasonic wave method

As the cracks generated by the expansion of reactive aggregate are the cause of deterioration due to ASR, the method used to investigate deterioration must be useful for evaluating the progress of fine cracks in concrete. **Figure 21** shows the relationship between the expansion and ultrasonic wave velocity obtained when specimens made of reactive aggregate were subjected to accelerated testing. Experimental conditions were a controlled temperature of 40°C, relative humidity of 100% and the testing period of 5-month

A decrease in ultrasonic wave velocity as the concrete expansion increases can be seen.

The Hanshin Expressway Corporation has been monitoring the progress of deterioration due to ASR inside bridge piers by measuring ultrasonic wave velocity since the 1980s. **Figure 22** shows an example of the inspection results (Kojima *et al*. 2000). The ultrasonic wave method was used to obtain data showing progress over time when visual inspection became difficult because the surface was covered with coating.

Using this method, efforts are being made to obtain

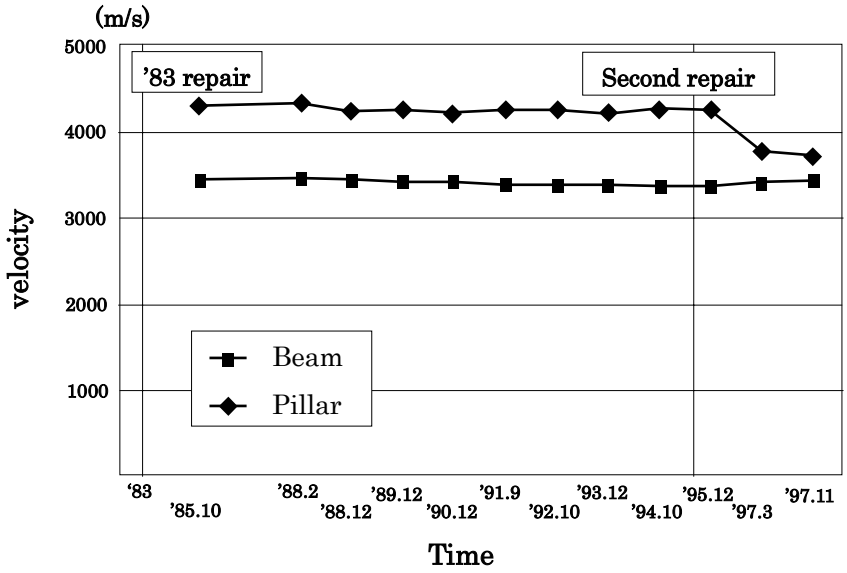

Fig. 22 Example of ultrasonic wave velocity over time.

information on deterioration due to ASR by focusing on the propagating waveform and energy, rather than just velocity as in the past. **Figure 23** shows the spectrum center of gravity of the obtained waveform, focusing on the ultrasonic propagating waveform. This accelerated test was carried out under the same conditions as described earlier. A decrease in the spectrum center of gravity with increasing expansion of the specimens can be observed.

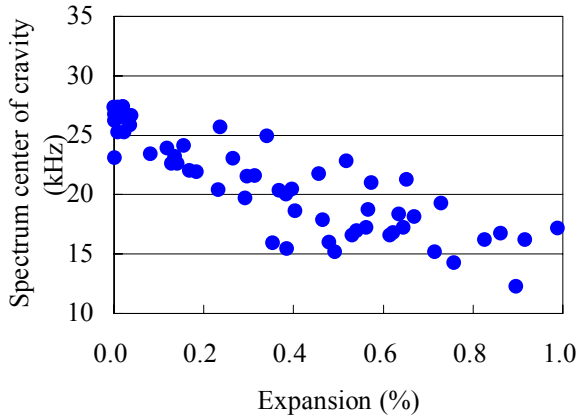

Fig. 23 Relationship between ultrasonic wave spectrum center of gravity and expansion.

Usually, the development of wide cracks is limited to the concrete cover if the steel confinement of bridge piers is in good condition. The features shown in **Fig. 24** can be seen in the propagating waveform under this condition, but these features change to those shown in **Fig. 25** when the cracks develop toward the interior as the confining reinforcements, such as stirrups, fracture. **Figure 26** shows the propagating waveforms recorded from a bridge pier with fractured stirrups. The wave amplitude through the fracture parts (confirmed at a later date by chipping inspection) was smaller than the sound pier.

In the oblique propagating method, it is necessary to suitably change the attachment locations of the ultrasonic terminals according to the position of the cracks, supports, accessories, and cover. It will also be necessary to accumulate data in future to allow quantitative evaluation of propagating waveforms because the damage condition of the surface coating and concrete surface can influence the results.

In order to quantitatively evaluate deterioration due to ASR from the data obtained with the ultrasonic wave method, it is necessary to accumulate more data with respect to the concrete mixture, aggregate type, moisture condition, and ultrasonic wave velocity. Because it is a relatively easy testing method, its use for research is expected to grow.

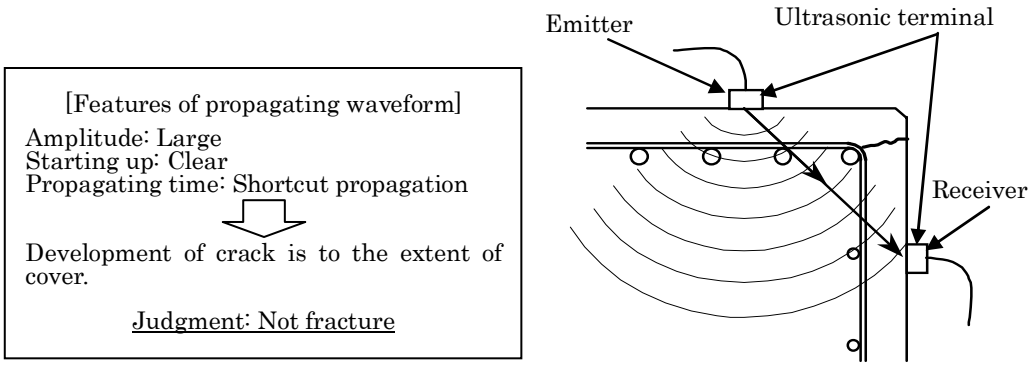

Fig. 24 Trend of propagating waveform (non-fracture case).

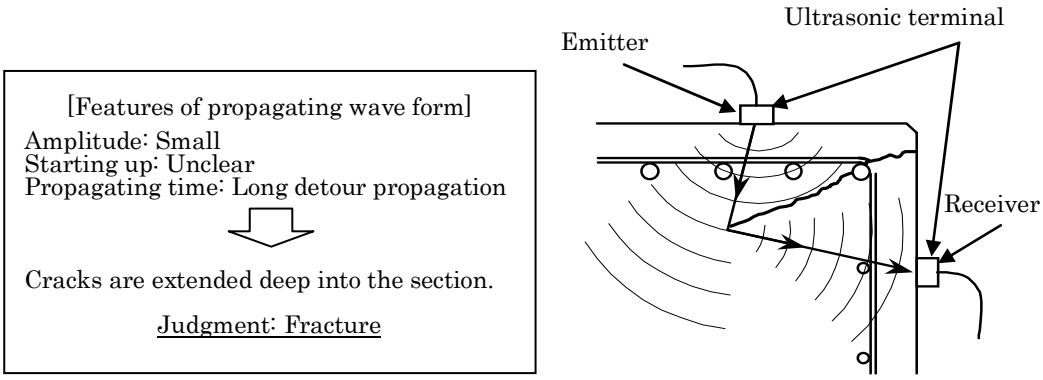

Fig. 25 Trend of propagating waveform (fracture case).

4.2 Electromagnetic testing method

When severe deterioration caused by ASR is present, steel bars may fail at the bent section inside the structure. If such damage is left unattended, it may advance further inside due to the lack of steel bar confinement, and eventually influence the safety of the structure. Therefore, proper investigation to determine the presence of steel bar fractures during maintenance and management of the structure is important.

The steel bar fractures in structures with ASR deterioration occur at bent sections. In such a case, an investigation of the foremost steel bars done by chipping out concrete may be considered, but protection against debris falling from high locations must be provided, resulting in very high cost. Therefore, a non-destructive inspection method is preferred. The application of the electromagnetic testing method as a non-destructive testing method for bent steel bars is being studied.

The principle of the electromagnetic testing method is the application of magnetic flux generated by an excitation coil of a sensor and reception of the reflected magnetic flux to detect fractures in steel through the detecting coil, as illustrated in **Fig. 27**.

The sensor consists of an excitation coil, a ferrite core, and a detecting coil, as shown in **Fig. 28**. The sensor uses a ferrite core to improve the strength of the mag-

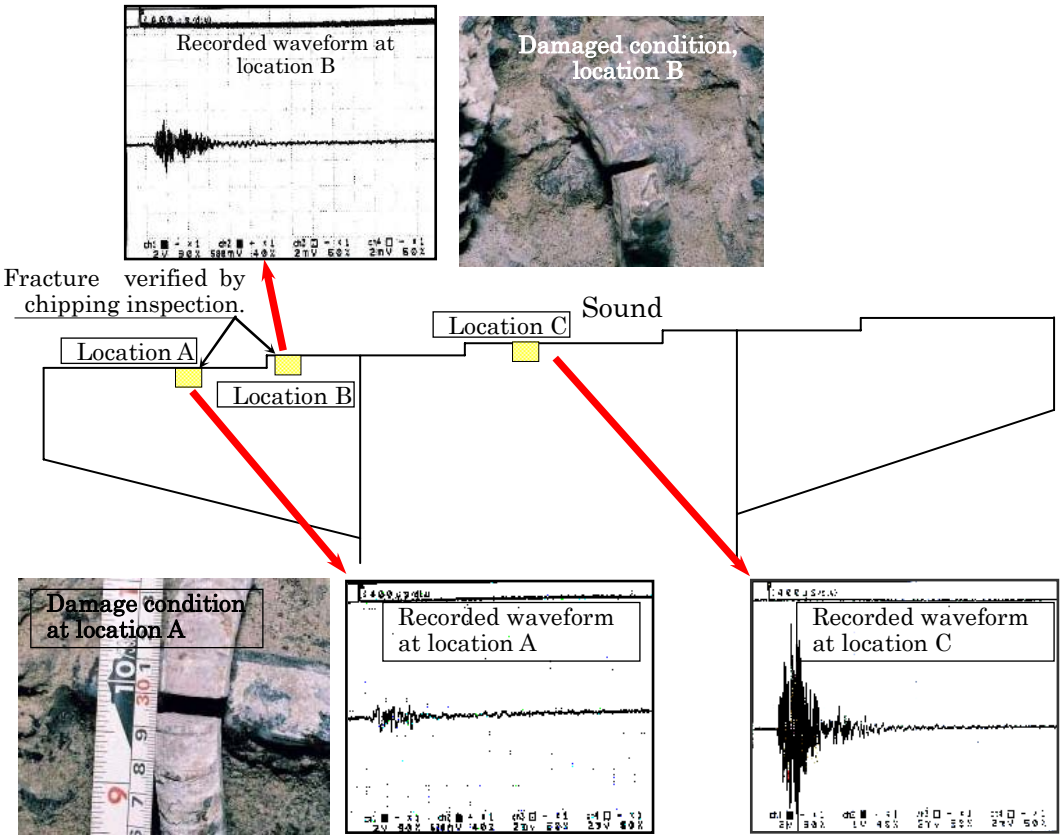

Fig. 26 Examples of recorded waveforms from existing bridge pier.

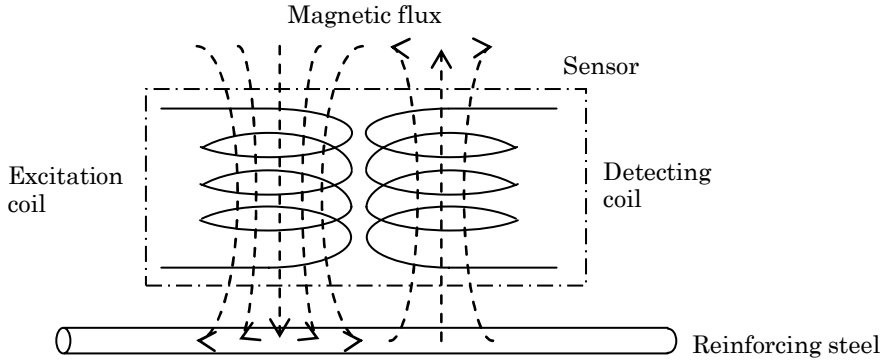

Fig. 27 Principle of electromagnetic testing method.

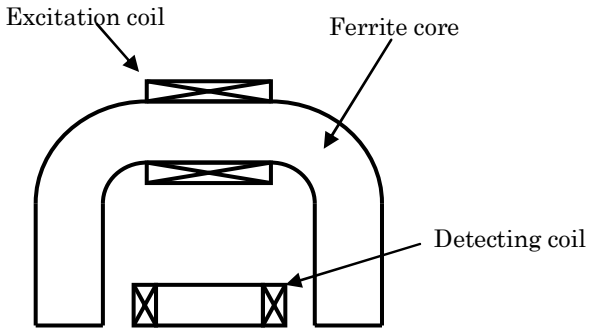

Fig. 28 Schematic view of sensor.

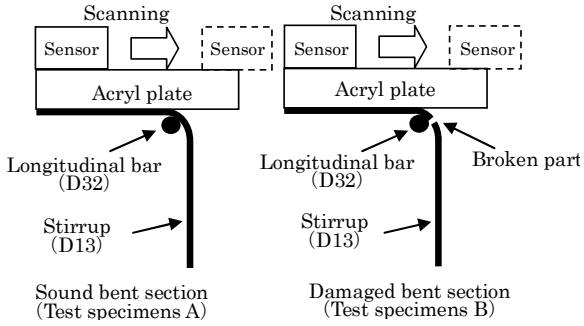

Fig. 29 Test specimens (bent section).

netic flux induced by the excitation coil, assuming cases when the distance between the sensor and reinforcing steel is large. A horseshoe shape is used for the coil to allow the closest possible proximity to the steel.

Figure 29 shows the arrangement used to measure the damage using a model specimen. The measured waveforms are influenced by bending processing, longitudinal bars, and so on. These unnecessary signals can be removed by mixing analysis. **Figure 30** shows the recorded waveforms obtained with the electromagnetic method applied to the stirrup through a 60 mm thick cover.

Since the inspector must judge whether or not the steel bar has been fractured by checking the waveform recorded with this method, research for the evaluation of waveforms in a more quantitative manner is under way. A method allowing examination through a cover up to 150 mm thick also needs to be developed, because the current maximum applicable depth of 100 mm is overly restrictive.

5. Strengthening methods for concrete structures damaged by ASR

5.1 Repair and strengthening

In the case of repairs, as a measure to control expansion, the use of water repellent agent to dissipate moisture inside the concrete is known to be effective for controlling the moisture content of concrete. The use of lithium ions to control ASR expansion has also been recognized as an effective method. However, when many steel bars are fractured, strengthening is often required because of the problem of possible over-loading caused by the reduced performance of the member or structure due to the weakened concrete strength and reduced modulus of elasticity caused by steel confinement fractures.

A flow chart detailing the strengthening approach is shown in **Fig. 31** (Concrete Library-124, 2005). This flowchart shows a standard measuring scenario of the strengthening approach for concrete structures damaged by ASR. If ASR is recognized as a result of investigation and diagnosis of the structure, and steel bar fractures are also confirmed, emergency measures shall be taken as required. The existing load carrying capacity

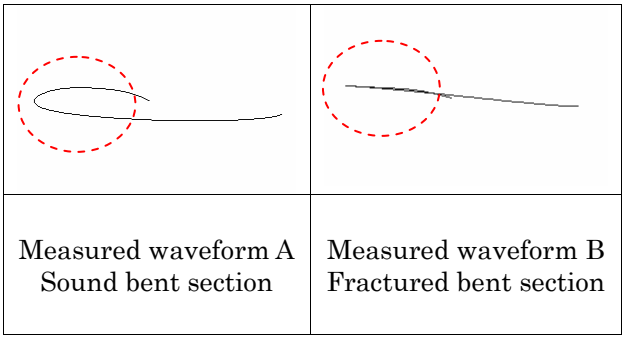

Fig. 30 Measured waveforms (Lissajou's figures) at bent section (distance between sensor and reinforcement:60 mm).

must be evaluated and then compared with the required value. Thereafter, estimation of future deterioration based on periodical inspection results, the design of scenario of measure, and the selection of a strengthening method are required. Prior to the strengthening work, calculation of the target load carrying capacity and confirmation of achievement of the target values should be conducted. Upon completion of the above, the actual strengthening work can be carried out. Following execution of the strengthening work, maintenance and management of the strengthened parts of the structure must be done through monitoring and periodical inspections, and records of these activities must be kept.

5.2 Strengthening confirmation test

The effect of strengthening when the method shown in the flowchart is selected (**Fig. 31**) must be confirmed. A strengthening test, using a large-scale specimen, is introduced to confirm the effect of the steel plate strengthening method. In the case of pier beams, steel plates cannot be bonded to the tension surface of the crown due to the presence of girder seats, and they can only be bonded to three faces, a compression surface and two side faces (**Fig. 32**). In this case, the concrete confining effect is expected to decrease and achievement of the designed effectiveness may not be possible.

Based on the above, loading tests using models of approximately half scale to confirm the strengthening effect of the method using steel plates on three sides

was conducted (Iwakawa *et al*. 2003).

5.2.1 Outline of experiment

The details of the tested specimens are listed in **Table 4**. Normal concrete was used for the sound specimen (Model 1), using 50-D16 (SD295, p = 0.37%) steel as main reinforcing steel bars and 3-D10 (SD295, p_w = 0.26%) steel for stirrups. On the other hand, test specimens were constructed to confirm the performance of steel plates replacing those of the main steel bars and the stirrups by assuming the fracture of reinforcing steels. Therefore, they do not contain main and shearing steel bars. Two specimens (Models 2 and 3) with steel plates bonded on all surfaces except the tension surface were prepared without steel bars. In order to simulate concrete deterioration due to ASR, a light-weight con-

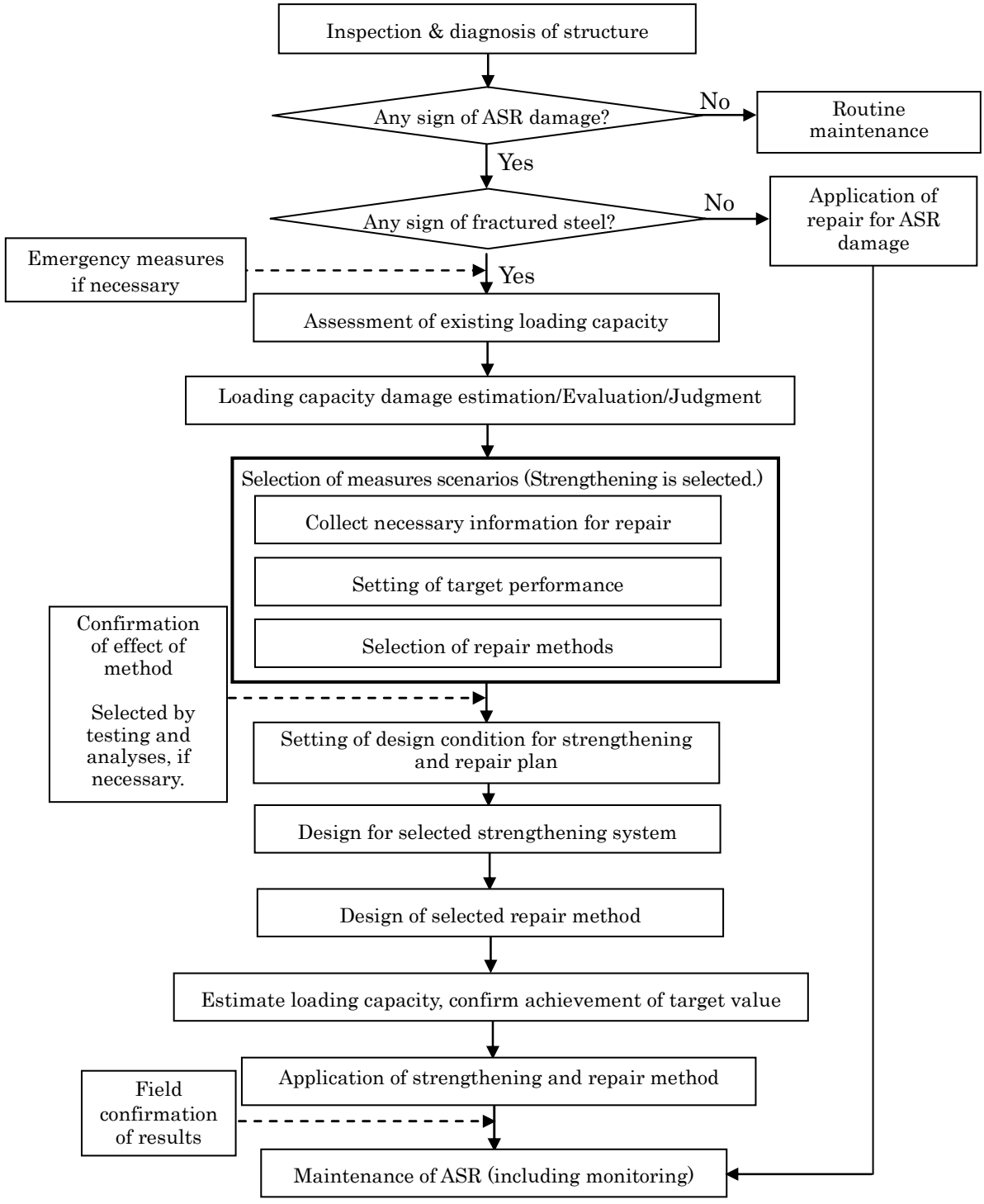

Fig. 31 Measure scenario flowchart.

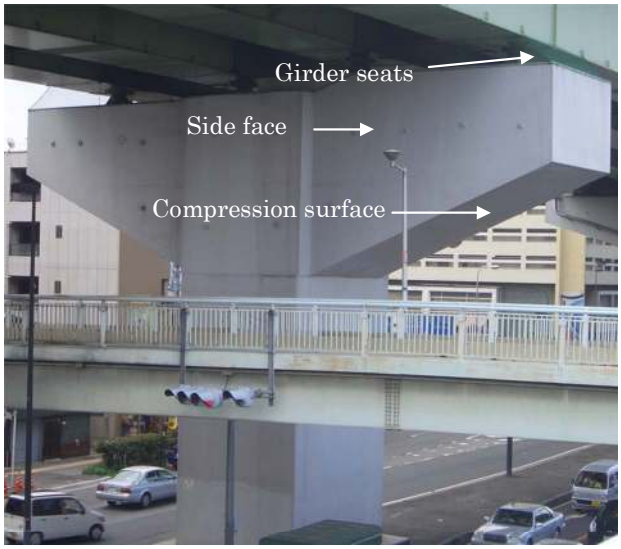

Fig. 32 Example of pier beam.

crete with reduced strength and reduced modulus of elasticity was used, and a steel plate thickness (t = 9mm, SM400) for representing approximately the same yield strength as that of a normal specimen was selected. There are two types of three-face strengthened specimens. The three surfaces of the Model 2 specimen are covered with steel plates, and its cross-sectional width varies in the middle, being wider at the pillar section of the pier. On the other hand, the Model 3 specimen is also strengthened with three steel plates, but its cross-sectional width is constant. The loading test was conducted in an upside-down configuration, simulating the crown of the pier section as the lower surface of the specimen.

5.2.2 Test results

The yield strength in bending was evaluated with the steel plates bonded to three surfaces on the beam that was damaged by ASR. Past research using small-scale specimens strengthened by bonded steel plates revealed that the ultimate yield strength in bending tended to be less than the calculated value obtained from fiber models. Therefore, the reduction coefficient of the bending yield strength for beams with steel plates on three surfaces was proposed with the following equation.

$$M_u^* = \alpha_1 \times M_u \quad (1)$$

M_u^* : Bending yield strength with three bonded steel plates
M_u : Bending yield strength, equivalent stress block method
α_1 : Reduction coefficient of bending yield strength (0.8 in this study)

Table 5 shows the test results. **Figure 33** shows the deflection with respect to loading. The measured maximum load, P_u, for the sound specimen (Model 1) and the specimen strengthened with three steel plates (Model 3) were nearly the same value, P_u = 5531 kN and 5688 kN, respectively. The Model 1 specimen

Table 4 Details of test specimens and loading conditions.

Model 1	Model 2	Model 3
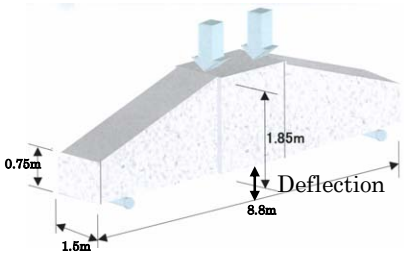	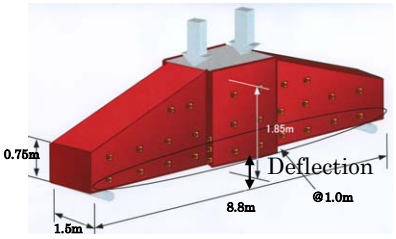	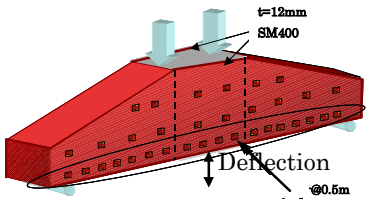
・Compressive strength f'_c = 30.6 N/mm² ・Young's modulus E_c= 29.4 kN/mm² ・Main reinforcement D16 (f_{py}= 349 N/mm²) × 50 bars (p = 0.37%) ・Longitudinal reinforcement D13 (f_{py} = 323 N/mm²) × 23 bars (p = 0.11%) ・Stirrup D10@110mm (f_{py}= 378 N/mm²) (pw = 0.26%)	・Compressive strength f'_c = 13.4 N/mm² ・Young's modulus E_c = 10.1 kN/mm² ・Non-reinforcement ・Steel plate t = 9 mm (f_{py} = 293 N/mm²) ・Pre-stressing bar ϕ 13 ・The flexural span and shear span widths are different.	・Compressive strength f'_c= 11.4 N/mm² ・Young's modulus E_c= 9.6 kN/mm² ・Non-reinforcement ・Steel plate t = 9 mm (f_{py} = 293 N/mm²) ・Pre-stressing bar ϕ 13 ・The flexural span and shear span widths are same.

Table 5 Test results.

Specimen	Ultimate Bending Yield Strength P_{ub}, kN (Calculated)	Maximum Load P_u, kN (Measured)	P_u/P_{ub}
Model 1	4305 †	5531	1.28
Model 2	4903 ††	745	0.15
Model 3	4903 ††	5688	1.16

† $P_{ub}=2\times Mu/a$

†† $P_{ub}=2\times Mu^*/a^*$

Mu : Bending yield strength

a : Shear span length for Model 1

Mu^* : Bending strength calculated by Eq. (1)

a^* : Shear span length for Models 2 and 3

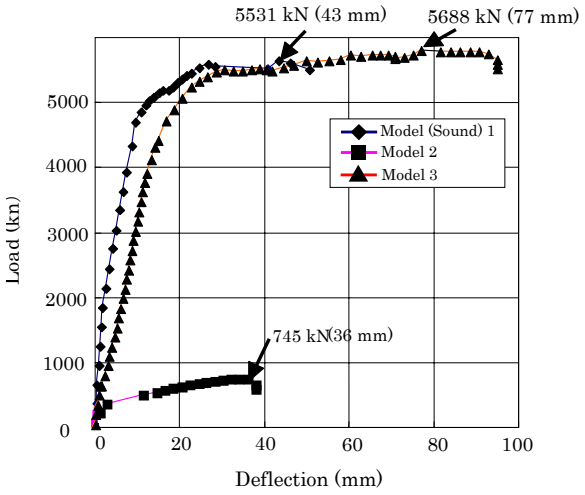

Fig. 33 Relationship between loading and deflection.

reached its ultimate loading when the average deflection at the loading point was approximately 50 mm. Model 3 specimen reached the same condition with approximately 90 mm deflection, indicating its satisfactory toughness. Based on these findings, the method of bonding steel plates on three surfaces consisting of both side faces and the compressive surface, of a non-reinforced concrete structure can be confirmed as being effective in providing equivalent yield strength and yielding excellent deflection characteristics compared to properly reinforced concrete structures. Thus the proposed steel plate strengthening method is effective for increasing the strength of concrete structures with steel bars fractured by ASR.

The calculated value of the bending yield strength, P_{ub}, of the sound specimen (Model 1) is P_{ub} = 4305 kN, and its ratio to the measured value is 1.28. Similarly, the calculated value for the Model 3 specimen is P_{ub} = 4903 kN, and its ratio to the measured value is 1.16. As these results indicate, the calculated ultimate bending yield strength can closely estimate the measured values.

Because of the variation in cross-sectional width at the center of the Model 2 specimen, stress concentration occurred in the area where the width changed. Consequently, the specimen failed abruptly as the stress was not evenly distributed on to the plates. Therefore, it is necessary to provide a means, such as a haunch, to properly distribute the stress to the steel plate when the cross-sectional width varies near the pillar and beam.

6. Maintenance of structures damaged by ASR

In many cases, the results of visual inspections are used to judge the stage of damage due to ASR. Not all structures affected by ASR necessarily develop visual deteriorations. Some of the structures retain their original appearance while others exhibit cracks and other abnormal conditions. However, structures that can be easily affected by moisture due to the development of cracks should be managed in one way or another to prevent further development of ASR.

When the damage further worsens, such as steel bar fractures and impact on third parties through falling debris, etc., it becomes necessary to compensate for the reduction in performance by taking appropriate measures. The possibility that steel bar rib shapes and bending radius may influence fractures has been pointed out, as well as the fact that the probability of bar fracture may be determined by the year of completion of the structure, because of the type of aggregate used at the time.

While the number of structures experiencing steel bar fractures is still small, and little research has been carried out to learn how ASR influences the load carrying performance of structures, it will be important in the future to establish methods for determining the safety of ASR-damaged structure.

7. Conclusions

(1) In piers with few reinforcing steels, many steel fractures at the bends of steels have been reported when deterioration due to ASR is severe at locations where the weather readily attacks the structures.

(2) The steel bar rib shape and the bending radius are considered to have a significant causal influence on steel bar fractures due to ASR

(3) It may be possible to determine the progress of deterioration that causes steel bar fractures by examining ultrasonic wave propagation characteristics. When the cover is less than 100 mm thick, the electromagnetic method may be used to determine the presence of steel bar fractures in a non-destructive manner.

(4) The method of bonding steel plates on three sur-

faces, both side faces and the compression surface excluding the tension surface, has been confirmed to be effective as a strengthening method for the beams of T shaped piers.

(5) There are many uncertainties concerning ASR at present, and research on the maintenance and management of concrete structures with the aim of finding reasonable measures through proper follow-up inspections without necessarily applying repairs or strengthening, will continue.

References

Concrete Library-124, (2005). "*State-of-the-Art Report on the Countermeasures for the Damage Due to Alkali-Silica Reaction*." Japan Society of Civil Engineers. (in Japanese)

Hundy, B. B. (1954). "Accelerated strain ageing of mild steel." *J. Iron Steel Inst*, 178, 34-38

Iwakawa, M., Seto, K., Mikata, Y., Maeda, S. and Miyagawa, T. "Experimental study on strengthening of ASR damaged RC beam using large specimens," *Concrete Structures Scenarios, JSMS*, October 2003. 51-56. (in Japanese)

Kojima, T., Hayashi, H., Kawamura, M. and Kuzume, K. (2000). "Maintenance of highway structures affected by alkali-aggregate reaction." *11th International Conference on* Alkali-Aggregate *Reaction*, 1159-1166.

Kuzume, K., Matsumoto, S., Minami, T. and Miyagawa, T. (2004). "Experimental study on breaking down of steel bars in concrete structures affected by alkali-silica reaction." *12th International Conference on Alkali-Aggregate Reaction in Concrete*, October 2004, 1162-1168.

Sasaki, K., Kawamura, M., Igarashi, H. and Miyagawa, T. (2005). "Report about cause investigation of steel bars damaged by alkali-silica reaction." *Concrete Structures Scenarios, JSMS*, October 2005,143-150. (in Japanese)

Notation:

a, a*: Shear span length
Ec : Young's modulus of elasticity
f_c : Compressive strength
f_{py} : Yield point strength
M_u : Bending yield strength
M_u* : Computed bending yield strength
P_u : Maximum load
P_{ub} : Ultimate bending yield strength
p : Reinforcement ratio
p_w : Stirrup reinforcement ratio
α_1 : Reduction coefficient of bending yield strength